

Quantum charge sensing using semiconductor device based on δ -layer tunnel junctions

Juan P. Mendez* and Denis Mamaluy*

Sandia National Laboratories

E-mail: jpmende@sandia.gov; mamaluy@sandia.gov

Abstract

We report a novel nanoscale device concept based on a highly doped δ -layer tunnel junction embedded in a semiconductor for charge sensing. Recent advances in Atomic Precision Advanced Manufacturing (APAM) processes have enabled the fabrication of devices based on quasi-2D, highly conductive, highly doped regions in semiconductor materials. In this work, we demonstrate that FET-based sensors utilizing APAM δ -layer tunnel junctions are ultrasensitive to the presence of charges near the tunnel junction, allowing the use of these devices for detecting charges by observing changes in the electrical current. We demonstrate that these devices can enhance the sensitivity in the limit, i.e. for small concentrations of charges, exhibiting significantly superior sensitivity compared to traditional FET-based sensors. We also propose that the extreme sensitivity arises from the strong quantization of the conduction band in these highly-confined systems.

Introduction

Sensors are indispensable components in our lives nowadays. Among all existing types of sensors, Field Effect Transistor (FET)-based sensors offer significant advantages for sensing:¹ they enable label-free electrical detection, provide real-time detection, can be small in size and weight, and,

most importantly, can be integrated on a chip. FET-based sensors have been widely reported for various applications, including the detection of cortisol, a hormone released in response to stress,² the SARS-CoV-2 virus associated with the COVID-19 pandemic,³ nucleic acids such as DNA or RNA,⁴ prostate-specific antigen (PSA), a key protein marker for prostate cancer,⁵ real-time detection of toxins in flowing water,⁶ as well as the measurement of pH⁵ and strain,⁷ among other applications.

The operation of conventional FET (CFET)-based sensors is similar to that of a MOSFET. CFET-based sensors consist of a source, drain, channel, insulator, and a sensing area, instead of the gate in MOSFETs. For example, in CFET-based sensors, the sensing area can be functionalized with receptor molecules that can trap the target molecules that we want to detect (see Figure 1 **a**). When the target molecules attach to the receptors, they act as a gate or, alternatively, they apply an effective voltage, depleting the channel and allowing electrons to flow from source to drain (see Figure 1 **b**). This results in an increase in current between the source and drain, with the magnitude of the current change being related to the concentration of the target molecule in the sample. This is how the concentration of target molecules is measured in biological applications using CFET-based sensors. However, CFET-based sensors suffer from sensitivity limitations, i.e. they require a minimum concentration of the target molecule in the sample to be detected and measured as a measurable current change. The sensitivity can be enhanced using tunnel FET (TFET)-based sensors (see Figure 1 **c**). In this case, when the target molecules attach to the sensing surface, it results in a lowering of the band structure of the channel. The signal, a measurable current change, is only received once the conduction band edge is lower than the valence band edge, enabling the band-to-band tunneling. Despite the enhanced sensitivity compared to its counterparts, the sensitivity still remains very low for low concentrations of the molecules in the sample, as it still requires a minimum concentration of molecules to bind to the sensing area to enable detectable band-to-band tunneling.

The sensitivity for TFET-based sensors can be approximated as $S \approx 10^{(\Delta Q \cdot q) / ((C_{ox} + C_{DL}) \cdot L \cdot SS)}$, where ΔQ is the charge change in the channel, SS is the subthreshold swing of the device, L is the

channel length, C_{DL} is the electrolyte double layer capacitance, and C_{OX} is the oxide capacitance.^{5,8} Therefore, S is essentially determined by the ratio of charge change to the total channel capacitive charge, which can only become non-negligible if those charges are comparable in magnitude. It is not surprising, therefore, that the best value of S for a TFET-based sensor to sense a single charge (i.e. for concentration of molecules $< 10^{-12}$ M) is just $S = 6.0 \times 10^{-3}$, assuming $SS = 20$ mV/dec, $C_{DL} = 4.7 \times 10^{-15}$ F/um, $C_{OX} = 1.4 \times 10^{-15}$ F/um and $L = 0.5$ um, which is also in agreement with previously reported sensitivity for TFET-based sensors.⁸ We propose that novel quantum FET-based sensors might enhance the sensitivity for detection at the limit, i.e. reaching a sensitivity of $S \gg 6.0 \times 10^{-3}$ for very low concentrations, and, consequently, open new opportunities for biological, chemical, radiation, and nuclear detection.

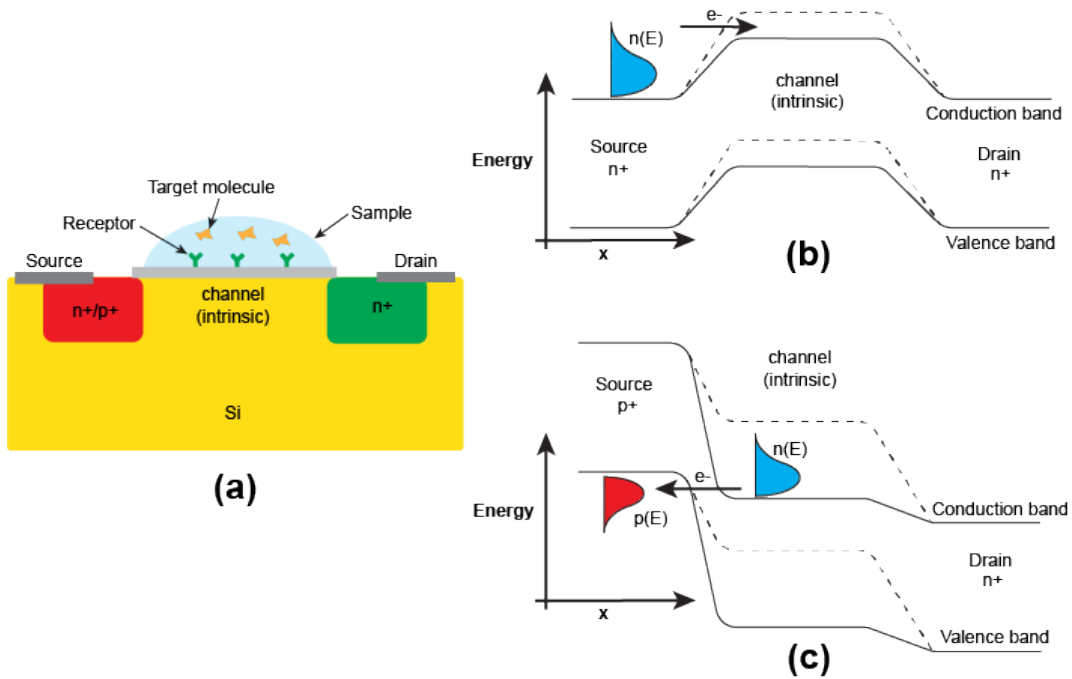


Figure 1: **a** Schematic representation of a FET-based sensor, n+/i/n+ for CFET and p+/i/n+ for TFET; **b** A typical band diagram for a CFET-based sensor (n+/i/n+); **c** A typical band diagram for a TFET-based sensor (p+/i/n+).

Recent advances in Atomic Precision Advanced Manufacturing (APAM) have enabled the creation of quasi-2D highly-doped regions, also known as δ -layers, in a semiconductor with single-atom precision^{9–13} and high conductivity.^{14–19} APAM is a manufacturing process used to incorpo-

rate dopants, such as P or B, at the atomic scale onto a Si surface using surface chemistry.^{18,20} This process involves several steps, as shown in Figure 2 **a** in a simplified way. For P-doped δ -layers embedded in silicon (Si: P δ -layer),²¹ the process starts with a Si surface, normally (100), fully passivated with H; with the help of the tip of a Scanning Tunneling Microscope (STM), H atoms are removed from the exact locations where dopants will later be incorporated; the Si surface is then exposed to a precursor gas, which contains the dopants, such as phosphene (PH₃)²⁰ for P dopants, followed by an annealing process to incorporate the dopants into the surface; finally, in the last step, an epitaxial Si is overgrown through a series of annealing processes to protect the planar structure and activate the dopants. APAM has various applications, including the exploration of novel electronic devices such as nanoscale diodes and transistors for classical computing and sensing systems,^{18,22–24} as well as the exploration of dopant-based qubits in silicon for quantum computing.^{25,26} In Ref.²³, the sensitive detection of single charges using a planar tunnel junction has been evaluated experimentally at cryogenic temperatures, where it has been demonstrated that the junction conductance strongly responds to the electrostatic field of a gate and to electron transitions of a quantum dot.

In this work, we propose a two-terminal APAM δ -layer tunnel junction (see Figure 2 **b**) as an ultra-sensitive device for charge sensing and explain the mechanism of the increased sensitivity in δ -layer tunneling junctions. These devices can offer significant advantages such as (i) they are exceptionally simple two-terminal devices; (ii) they are extremely small-size, on the order of 10 nm; and (iii) they are suitable for integration with CMOS technology. As motivation, Figure 2 **c** includes an example of an APAM device for detecting molecules in biological applications. This device consists of two δ -layers, separated by an intrinsic gap. The sensing area, above the tunnel junction, is functionalized with a type of receptor molecule, which selectively attracts the target molecule to be measured or detected. Once the target molecule is attached to the receptor, it induces the presence of charges near the tunnel junctions. These charges can be measured by changes in the current between the source and drain.

We demonstrate in this work that APAM δ -layer tunnel junctions can easily detect single

charges near the tunnel junction by observing measurable changes in the electrical current. We also show theoretically that these devices exhibit sensitivity superior to that of CFET and TFET-based sensors in the low-charge concentration limit. Finally, we prove that the extreme sensitivity arises from the strong quantization of the conduction band in these highly-confined δ -layers.

Results and discussion

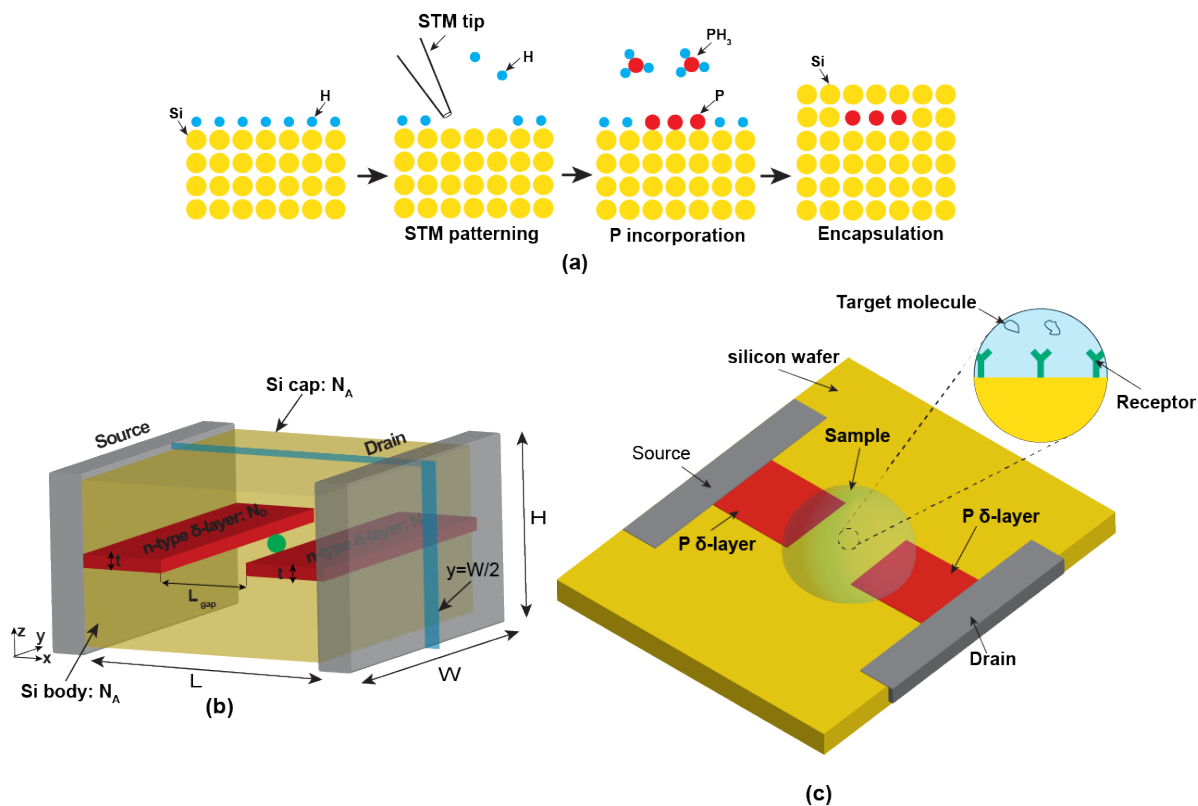


Figure 2: **a** Key steps in the Atomic Precision Manufacturing (APAM) process. **b** Schematic of the computational device (APAM δ -layer tunnel junction) used in our simulations, consisting of two very thin, highly n-type-doped layers separated by an intrinsic semiconductor gap and embedded in silicon. **c** Example of an APAM FET-based sensor for biological application. In **c**, the sensing area, above the tunnel junction, is functionalized with a receptor molecule that can selectively trap the target molecule.

The first question that we would like to address is whether δ -layer tunnel junctions are sensitive to the presence of a very low number of charges near the tunnel junction. In order to answer this question, we first look at whether the tunneling current changes when a single (negative/positive)

charge is present near the junction. For the simulations, we adopt the structure of the δ -layer tunnel junction shown in Figure 2 **b**, which consists of two very conductive, thin, highly n-type-doped (e.g., P) layers separated by an intrinsic semiconductor gap and embedded in silicon. We consider a δ -layer with a thickness of $t = 1.0$ nm and with a donor sheet doping density of $N_D = 1.0 \times 10^{14} \text{ cm}^{-2}$ ($N_D^{(2D)} = t \times N_D^{(3D)}$), and a tunnel junction length of $L_{gap} = 10$ nm. The Si body and Si cap are lightly doped with acceptors, with a doping density of $N_A = 5.0 \times 10^{17} \text{ cm}^{-3}$. Further details of the computational simulations can be found in the Methods section.

Figure 3 shows the tunneling-current contour map when a positive/negative charge is located at different positions (x,z) in the middle plane of the device ($y=W/2$), shown in Figure 2 **b**, at 4 and 300 K, when a voltage of 1 mV is applied between the source and drain. These results indicate that the presence of either a negative/positive charge near the tunnel junction indeed strongly affects the tunnel rate in δ -layer tunnel junctions. A negative charge increases the tunneling current, while a positive charge decreases it, demonstrating that our APAM device is indeed suitable for charge sensing. The maximum current change occurs when the charge is present in the center of the tunnel junction: at 4 K, with a decrease of up to 0.17 nA for a positive charge and an increase of up to 1.86 nA for a negative charge; at room temperature, with a decrease of up to 15.1 nA for a positive charge and an increase of up to 24.6 nA for a negative charge. However, most importantly, the tunneling rate not only changes when the charge is located between the δ -layers, but also when it is located outside the δ -layers, which is an important result if we want to use this device for charge sensing. These results also suggest that the impact of the electrical charge on the current diminishes as the charge moves farther away from the tunnel junction, indicating that the δ -layer detects the presence of the charge when it is near the tunnel junction, but does not detect it when the charge is very far away (e.g., when the charge is at position $x = 12$ nm and $y = 3$ nm). In a semiclassical picture, the increase/decrease of the tunneling rate caused by the presence of a negative/positive charge can be understood because a negative charge decreases the effective barrier height of the tunnel junction by creating discrete states in the junction region, whereas a positive charge increases the effective barrier height by depleting states within the junction region.

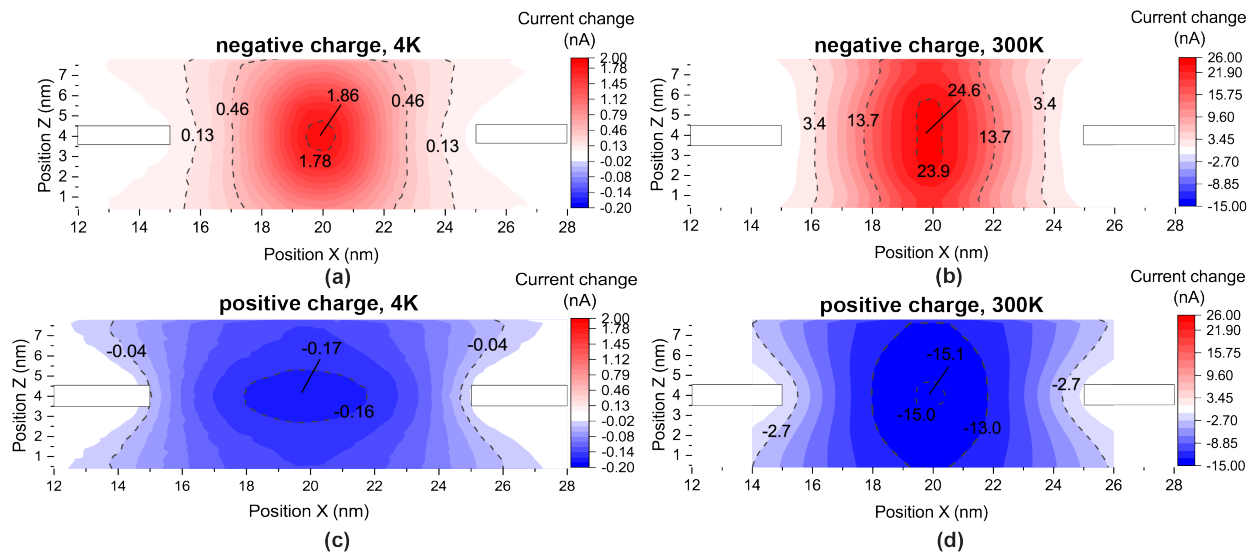


Figure 3: Contour maps of the tunneling current change due to the presence of a single negative charge at different positions (x,z) in the middle plane of the device $(y=W/2)$ at 4 K in **a** and at 300 K in **b**, as well as for a single positive charge at 4 K in **c** and at 300 K in **d**. A voltage of 1 mV is applied between the source and drain. The nominal tunneling current (i.e. without charges near the tunnel junction) is around 0.27 nA at 4 K and 28.5 nA at 300 K.

Next, in Figure 4, we evaluate the sensitivity of the device. The sensitivity S , defined as the ratio of the change in current caused by the presence of a single charge to the nominal current, is expressed as $S = I_{\text{with charge}}/I_{\text{nominal}} - 1$, where $I_{\text{with charge}}$ refers to the current through the device when a single charge is present near the tunnel junction and I_{nominal} refers to the current of the device in the absence of charges near the tunnel junction. This metric indicates how much the tunneling rate changes relative to the nominal current of the device. Figure 4 indicates that the device exhibits very high sensitivity, especially for negative charges at low temperatures. At 4 K, we obtain a maximum sensitivity of 6.9 for sensing a negative charge in the middle of the tunnel junction, while the sensitivity for a positive charge is around 0.64. Similarly, the sensitivity decreases as the charge moves farther away from the center of the tunnel junction. As expected, these results also show that the sensitivity decreases with the increase in temperature due to the contribution of the thermionic emission. At room temperature, we obtain a maximum sensitivity of 0.86 for sensing a negative charge in the middle of the tunnel junction, while the sensitivity for a positive charge is 0.53. There are two contributions to the total current in these systems: the thermionic emission

($j_{\text{thermionic}} = AT^2 \exp(-E_b/k_bT)$, where E_b is the barrier energy) and the tunneling current. The former corresponds to high-kinetic-energy electrons, with energies higher than the barrier energy at the junction, which can pass through tunnel junction without tunneling; the latter corresponds to electrons with energies lower than the barrier energy that can pass through the barrier via tunneling. If we approximate the sensitivity as $S = \Delta I_{\text{due to charges}} / (I_{\text{thermionic}} + I_{\text{tunneling}})$, where $I_{\text{thermionic}}$ and $I_{\text{tunneling}}$ are the nominal current contributions due to the thermionic emission and tunneling, respectively, and $\Delta I_{\text{due to charges}}$ is the current change due to the presence of charges, we observe that sensitivity can rapidly decrease with temperature as $I_{\text{thermionic}}$ increases with temperature. Despite the decrease in sensitivity with temperature, these results also demonstrate that our APAM FET-based sensor achieves superior sensitivity compared to CFET and TFET-based sensors even at room temperature. The maximum sensitivity of our device is around $S = 0.86$ at 300 K, which is significantly larger than the theoretical sensitivity of TFET sensors, typically $S \sim 10^{-3}$ for low concentrations of charges.

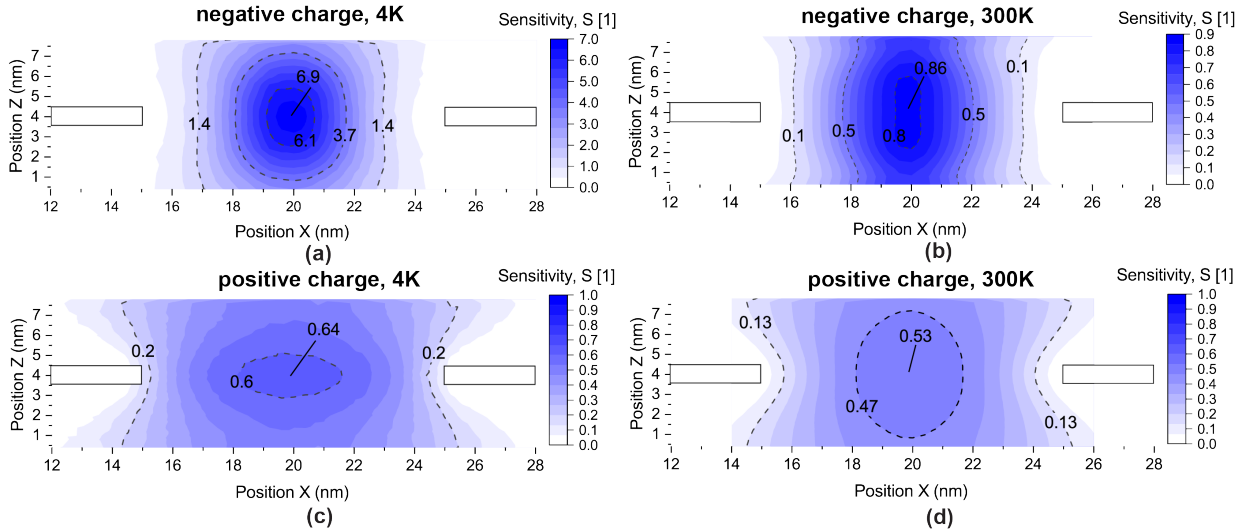


Figure 4: Sensitivity of the device due to the presence of a single negative charge located at different positions (x,z) in the middle plane of the device ($y=W/2$) at 4 K in **a** and at 300 K in **b**, as well as for a single positive charge at 4 K in **c** and at 300 K in **d**. A voltage of 1 mV is applied between the source and drain. The device dimensions are: $L = 40$ nm, $W = 15$ nm, $H = 8$ nm, and $t = 1$ nm.

To achieve higher sensitivity for positive charges, comparable to that of negative charges, p-

type δ layers can be used instead of n-type δ layers. Additionally, we also note that because the effects on the current due to the presence of a negative charge and a positive charge are dissimilar in magnitude, this device is also suitable for infrared photon detection, wherein the impact of a photon on the sensing area of the device results in a cascade of electron-hole pairs. An electron-hole pair cloud can be modeled as a single dipole with total charge Q and a dipole moment l . In our previous work,²⁷ we found that dipoles with sufficiently large moments can significantly affect the tunneling current in δ -layer tunnel junctions, depending on the dipole orientation with respect to the δ -layer system.

We next investigate how far the proposed device can sense the presence of charges. Figure 5 shows the sensitivity of the device for different positions of a single negative charge located at a distance d from the tunnel junction (see the inset in figure a) at both temperatures, 4 K and 300 K. The applied voltage between the source and drain is 1 mV. Due to limitations in the computational resources, in this simulation, we use a smaller device width of $W = 10$ nm, while adopting a larger device height of $H = 15$ nm, with the δ -layers positioned asymmetrically 5 nm from the bottom of the device. At 4 K, the results indicate that the sensitivity initially decays nearly-exponentially with the distance from the δ -layer tunnel junction at first, but then, at distances greater than 5 nm, the sensitivity starts reducing at a much slower rate, maintaining a relatively high value $S \sim 1$. At 300 K, the sensitivity is roughly constant up to a distance of 3 nm, then it decays nearly-exponentially with the distance. Interestingly, the rate of the sensitivity decay at short distances is higher at 4K than at 300 K, while it is the opposite at long distances. Thus, we can conclude that δ -layer tunnel junctions can detect charges over longer distances at lower temperatures, specifically at 4 K. We also note that narrower devices with stronger confinement exhibit greater sensitivity, specifically at 4 K, as we can conclude by comparing the results from Figures 4 and 5; the maximum sensitivity for a device width of 15 nm is 6.9, while it is around 12.5 for a device width of 10 nm at 4 K. This enhancement in sensitivity is due to the size quantization effects in δ -layers systems. A similar observation has been observed in other systems, such as nanowires, in which it has been demonstrated that the sensitivity decreases as the diameter of the nanowire decreases.²⁸

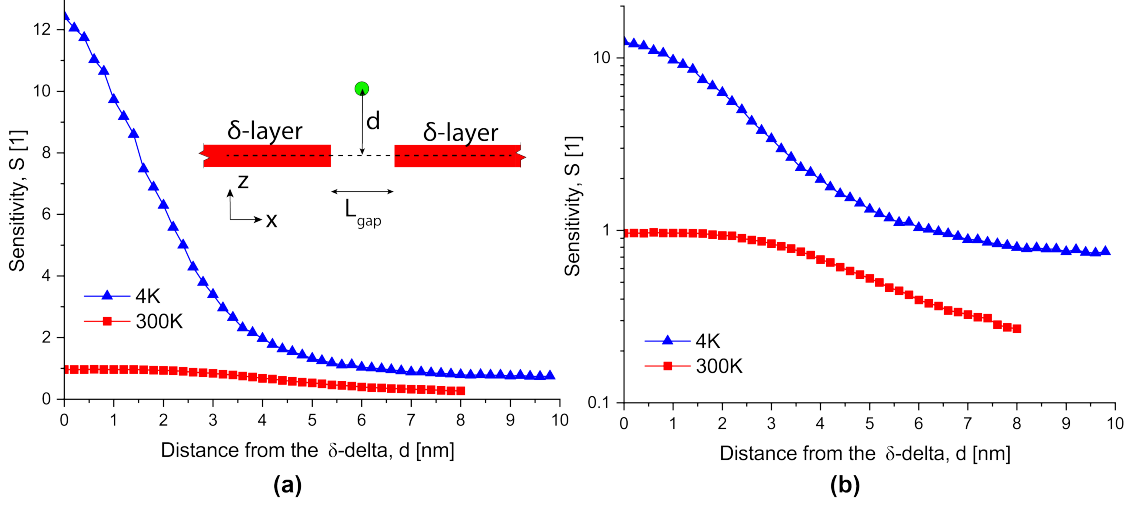


Figure 5: Sensitivity of the device to the presence of a single negative charge located at different distances d from the δ -layers, along the line $(x, y, z) = (L/2, W/2, d)$, at both temperatures 4 and 300 K. **a** Linear scale; **b** Log scale. The inset in **a** displays the schematic representation of a tunnel junction and a charge located at a distance d from the δ -layer. A voltage of 1 mV is applied between the source and drain. The device dimensions are: $L = 40$ nm, $W = 10$ nm, $H = 15$ nm, and $t = 1$ nm.

Figure 6 **a** shows the sensitivity of the device as a function of the thickness of the δ -layer for both temperatures, 4 K (left panel) and 300 K (right panel), and at two applied voltages between the source and drain of 1 mV and 100 mV. For this study, a single (negative) charge is placed in the middle of the device, between the δ -layers, at the coordinates $(x, y, z) = (L/2, H/2, W/2)$, and we evaluate how the tunnel current changes for various thicknesses. One can clearly observe from these results that the maximum sensitivity is achieved for thinner δ -layers, after which the sensitivity decreases as the thickness increases. One can also note from these results that at higher temperatures the sensitivity is higher at lower voltages. These results demonstrate that thinner δ -layers are more sensitive than thicker ones and, as we discuss in the following, the higher sensitivity for thinner δ -layers arises from the strong quantization of the conduction band in these highly-confined systems, which is the result of the confinement of the dopants in the z -direction (see Figure 2 **b**).

In our previous work, Refs.^{29,30}, we found that the conduction band structure of δ -layers is strongly quantized, resulting in quasi-discrete states in the low-energy conduction band. A

schematic representation of the conduction band quantization for δ -layers is shown in Figure 6 **b**. The quantized states are represented in the figure with thin stripes in the low-energy conduction band, whereas the continuous states are represented with thick stripes. The Fermi-Dirac distribution determines the occupancy of states, distinguishing between occupied and unoccupied states. In Refs.^{29,30}, we also found that the number of quantized states, as well as the corresponding splitting energy between them, are strongly dependent on both the δ -layer thickness t and the doping density N_D . We indeed found that, as we increase the thickness of the δ layer and maintain constant the total charge (i.e. fixing constant the 2D doping density), the splitting energy between them becomes smaller, resulting in less quantization of the conduction band (see Figure 6 **c**). These previous results, together with the results from Figure 6 **a**, demonstrate that thinner δ -layers are more sensitive than thicker ones due to the stronger quantization of the conduction band. As the thickness of the δ -layer increases, the conduction band becomes less quantized. This reduces the deviation of the tunneling rate from the ideal rate, thereby decreasing the sensitivity of the δ -layer to detect charges near the tunnel junction. Finally, we note that the proposed extreme sensing mechanism is reminiscent of the charge sensing (see Ref.³¹) using single-electron transistors (SETs),³² but without the need in Coulomb blockade effect and with the quasi-discrete energy levels located in the "source" and "drain", instead of the (unnecessary for δ -layers) "island", as shown in Figure 6 **b**.

As demonstrated, APAM tunnel junctions are very sensitive to presence of charges, making the device very suitable for sensing applications that involve charges. Examples of these applications are: (i) biomolecular sensing; (ii) radiation sensor; (iii) microscopes (for spectroscopy); (iv) brain-computer interface (BCI) applications, to unlock and interpret the brain's electrical signals with high spatial resolution and the capability to capture small signals.

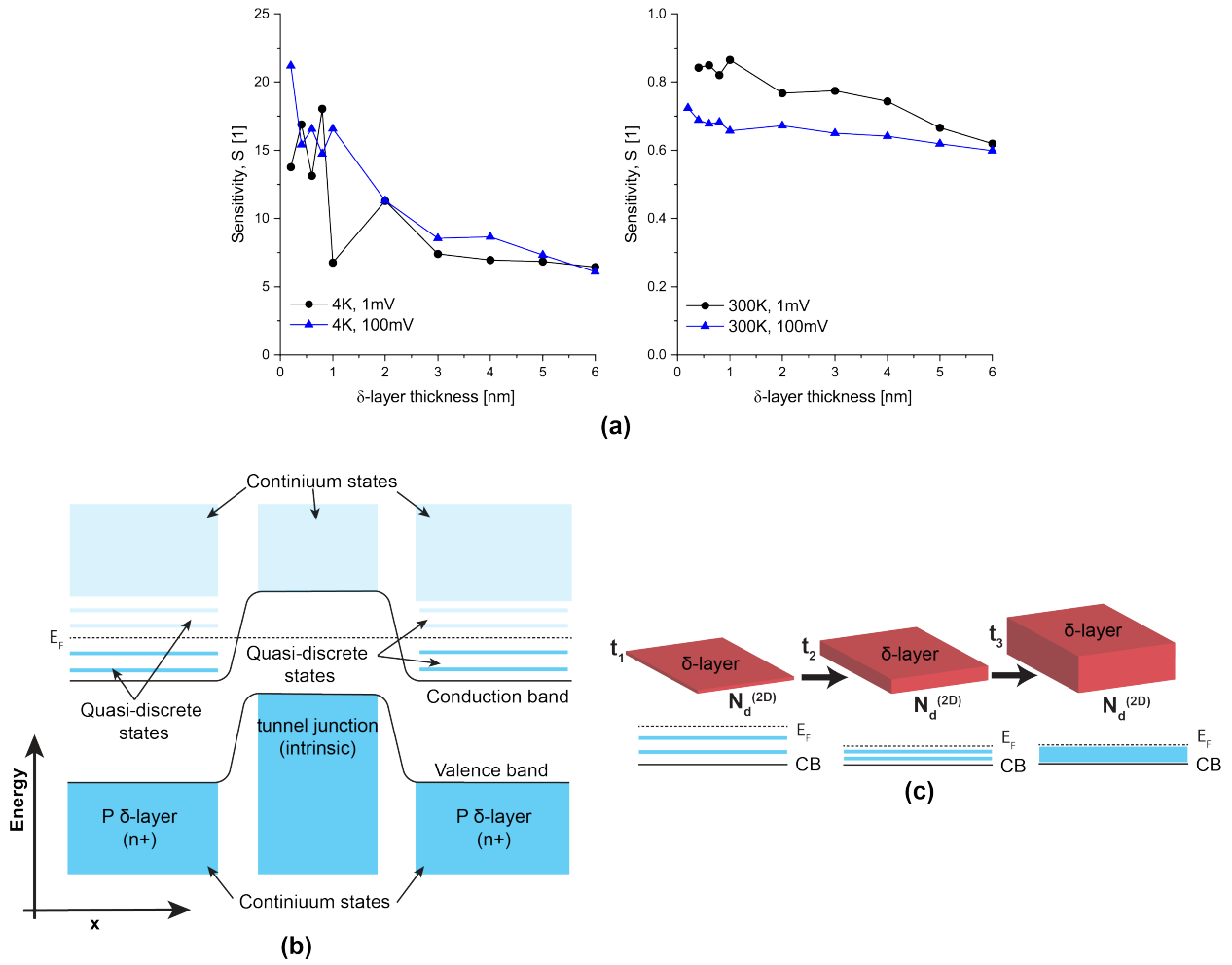


Figure 6: **a** Sensitivity vs. δ -layer thickness study when a single negative charge is placed between the δ -layers. **b** Schematic representation of the band structure in real space for δ -layers tunnel junctions in a semiconductor; The quantized states are represented in the figure with thin stripes in the low-energy conduction band, whereas the continuous states are represented with thick stripes. **c** Schematic representation of the effect of the δ -layer thickness on the conduction band structure.

Conclusions

In this work, we have demonstrated the extreme sensitivity of APAM FET devices, based on δ -layer tunnel junctions embedded in a semiconductor, for charge sensing in the low-concentration limit, i.e. for detecting single charges. They can open new opportunities in biological, chemical and radiation sensing. These devices also offer the following advantages compared to traditional FET-based or TFET-based sensors: (i) the exceptional simplicity of two-terminal devices; (ii) very small device dimensions, on the order of 10 nm by 10 nm, which also allow a high density of sensing elements; and (iii) the readiness of integration with CMOS technology. These advantages could make these simple and potentially high-density charge sensors particularly suitable for *charge sensing array* devices, including scanning types, where signals from multiple sensing cells in the sensor array would be processed "on-site" using a neuromorphic architecture to provide real-time analysis, enhance the sensitivity, selectivity and provide the capability to detect multiple target elements.⁶

Specifically, we have investigated how the tunneling current is affected by the presence of a single positive/negative charge near the tunnel junction in a two-terminal P-doped δ -layer tunnel junction embedded in silicon at cryogenic and room temperature. We found that the presence of a single charge strongly affects the tunneling current, particularly for negative charges, resulting in a high sensitivity of these devices. We have also demonstrated that these devices can enhance the sensitivity in the limit, exhibiting superior sensitivity compared to CFET and TFET-based sensors. The sensitivity metric, defined as the ratio of the current change to the nominal change, indicates how much the tunneling rate changes relative to the nominal current of the device. In fact, our results show that our APAM FET-based sensor achieves superior sensitivity: the maximum sensitivity is around 6.9 at 4 K and 0.86 at 300 K for a single negative charge, which is significantly higher than the theoretical upper bound of sensitivity for TFET-based sensors, typically $S = 6 \times 10^{-3}$ for low concentrations of charges. As exhibited in this work, the sensitivity of these devices at low temperature can be also enhanced by reducing the width of the δ -layers: for a δ -layer width of 10 nm, the sensitivity increases up to approximately 12.5 at 4 K. We have also demonstrated

that APAM tunnel junctions can effectively sense charges far from the tunnel junction, specifically at 4 K. Finally, we have proposed and demonstrated that the extreme sensitivity to the presence of charges arises from the strong quantization of the conduction band in these highly confined systems.

Methods

The simulations in this work are conducted using the open-system charge self-consistent Non-Equilibrium Green Function (NEGF) Keldysh formalism,^{33,34} together with the Contact Block Reduction (CBR) method³⁵⁻⁴² and the effective mass theory. The CBR method allows a very efficient calculation of the density matrix, transmission function, etc. of an arbitrarily shaped, multiterminal two- or three-dimensional open device within the NEGF formalism and scales linearly $O(N)$ with the system size N . As validation, in our previous works,^{29,43} we demonstrated a very good agreement with experimental electrical measurements for Si: P δ -layer systems,^{14,44-46} proving an excellent reliability of this framework to investigate δ -layer systems. Similarly, our published results in Refs.^{27,30}, without fitting parameters, agree remarkably well with the most recent experimental data for tunnel junctions in these systems.⁴⁷

Within this framework, we solve self-consistently the open-system effective mass Schrödinger equation and the non-linear Poisson equation.^{35,38,41} We employ a single-band effective mass approximation with a valley degeneracy of $d_{val} = 6$. For the charge self-consistent solution of the non-linear Poisson equation, we use a combination of the predictor-corrector approach and Anderson mixing scheme.^{39,41} First, the Schrödinger equation is solved in a specially defined closed-system basis taking into account the Hartree potential $\phi^H(\mathbf{r}_i)$ and the exchange and correlation potential $\phi^{XC}(\mathbf{r}_i)$.⁴⁸ Second, the local density of states (LDOS) of the open system, $\rho(\mathbf{r}_i, E)$, and the electron density, $n(\mathbf{r}_i)$, are computed using the CBR method for each iteration. Then, the electrostatic potential and the carrier density are used to calculate the residuum F of the Poisson

equation

$$\|\mathbf{F}[\phi^H(\mathbf{r}_i)]\| = \|\mathbf{A}\phi^H(\mathbf{r}_i) - (\mathbf{n}(\mathbf{r}_i) - \mathbf{N}_D(\mathbf{r}_i) + \mathbf{N}_A(\mathbf{r}_i))\|, \quad (1)$$

where \mathbf{A} is the matrix derived from the discretization of the Poisson equation, and \mathbf{N}_D and \mathbf{N}_A are the total donor and acceptor doping densities arrays, respectively. If the residuum is larger than a predetermined threshold ε , the Hartree potential is updated using the predictor-corrector method, together with the Anderson mixing scheme. Using the updated Hartree potential and the corresponding carrier density, the exchange-correlation is computed again for the next step, and an iteration of the Schrödinger-Poisson equations is repeated until the convergence is achieved with $\|\mathbf{F}[\phi^H(\mathbf{r}_i)]\| < \varepsilon = 5 \times 10^{-6}$ eV. In our simulations, we have utilized a 3D real-space model, with a discretization size of 0.2 nm along all directions, thus with about 10^6 real-space grid points, and up to 4,000 energy points were used. The CBR algorithm automatically ascertains that out of more than 1,000,000 eigenstates only about 1000 ($< 0.1\%$) of lowest-energy states is needed, which is generally determined by the material properties (e.g. doping level) and the temperature of the system, but not the device size. We have also employed the standard values of the inertial effective mass tensor for electrons, $m_l = 0.98 \times m_e$, $m_t = 0.19 \times m_e$, and the dielectric constant of Silicon $\varepsilon_{Si} = 11.7$. Further details of the methodology to study these systems can be found in our previous publications.^{29,30,42,49}

The computational device used in this work, shown in Figure 2 **b**, consists of a semi-infinite source and drain, in contact with the channel of length L . By using the NEGF open boundary conditions, the source and drain represent a way to extend the channel into infinity along the x-axis. Therefore, the source and drain have the same properties as the channel. The channel is composed of a lightly doped Si body and Si cap and two very thin, highly n-type (e.g., P) doped layers separated by an intrinsic gap of length L_{gap} . If not specified otherwise in the manuscript, the channel length L is set to $30 \text{ nm} + L_{gap}$ to avoid boundary effects between the source and drain contacts, the tunnel gap length L_{gap} is 10 nm, the device height H is 8 nm, and the device width W is 15 nm, with an effective width of 13 nm for the δ -layers, to minimize size quantization effects on the conductive properties.³⁰ Similarly, we have considered a thickness of δ -layer of $t = 1$ nm, a

sheet doping density of $N_D = 10^{14} \text{ cm}^{-2}$ ($N_D^{(2D)} = t \times N_D^{(3D)}$) in the δ -layers, and a doping density of $N_A = 5 \times 10^{17} \text{ cm}^{-3}$ in the Si cap and Si body. These doping densities and dimensions are of the order of published experimental work.^{20,47,50–52} In our simulations, the negative/positive charge is modeled by approximating a point charge with a density of (positive or negative) $4.6 \times 10^{21} \text{ cm}^{-3}$ homogeneously distributed in a total volume of $(0.6 \text{ nm})^3$. The final spatial distribution of the total charge will be dictated by the self-consistent solution of the open-system Schrödinger and Poisson equations. Finally, we have neglected inelastic scatterings in our simulations. At the cryogenic temperature of 4.2 K, inelastic scattering can be neglected^{14,53} since phonon are effectively freeze-out; at room temperature, we assume than the impact of thermionic emission on the sensitivity is greater than that of inelastic scattering. However, further studies need to be done to elucidate the role of inelastic scattering on electron transport at room temperature.

Data availability

The datasets used and/or analyzed during the current study are available from the corresponding authors on reasonable request.

Acknowledgement

The authors are deeply grateful to John Wagner for his encouragement and support of this work. Sandia National Laboratories is a multission laboratory managed and operated by National Technology and Engineering Solutions of Sandia, LLC., a wholly owned subsidiary of Honeywell International, Inc., for the U.S. Department of Energy’s National Nuclear Security Administration under contract DE-NA-0003525. This paper describes objective technical results and analysis. Any subjective views or opinions that might be expressed in the paper do not necessarily represent the views of the U.S. Department of Energy or the United States Government.

References

- (1) Dai, C.; Liu, Y.; Wei, D. Two-Dimensional Field-Effect Transistor Sensors: The Road toward Commercialization. *Chemical Reviews* **2022**, *122*, 10319–10392, PMID: 35412802.
- (2) Sheibani, S.; Capua, L.; Kamaei, S.; Akbari, S. S. A.; Zhang, J.; Guerin, H.; Ionescu, A. M. Extended gate field-effect-transistor for sensing cortisol stress hormone. *Communications Materials* **2021**, *2*, 10.
- (3) Seo, G.; Lee, G.; Kim, M. J.; Baek, S.-H.; Choi, M.; Ku, K. B.; Lee, C.-S.; Jun, S.; Park, D.; Kim, H. G.; Kim, S.-J.; Lee, J.-O.; Kim, B. T.; Park, E. C.; Kim, S. I. Rapid Detection of COVID-19 Causative Virus (SARS-CoV-2) in Human Nasopharyngeal Swab Specimens Using Field-Effect Transistor-Based Biosensor. *ACS Nano* **2020**, *14*, 5135–5142, PMID: 32293168.
- (4) Hwang, M. T.; Heiranian, M.; Kim, Y.; You, S.; Leem, J.; Taqieddin, A.; Faramarzi, V.; Jing, Y.; Park, I.; van der Zande, A. M.; Nam, S.; Aluru, N. R.; Bashir, R. Ultrasensitive detection of nucleic acids using deformed graphene channel field effect biosensors. *Nature Communications* **2020**, *11*, 1543.
- (5) Gao, X. P. A.; Zheng, G.; Lieber, C. M. Subthreshold Regime has the Optimal Sensitivity for Nanowire FET Biosensors. *Nano Letters* **2010**, *10*, 547–552, PMID: 19908823.
- (6) Maity, A.; Pu, H.; Sui, X.; Chang, J.; Bottum, K. J.; Jin, B.; Zhou, G.; Wang, Y.; Lu, G.; Chen, J. Scalable graphene sensor array for real-time toxins monitoring in flowing water. *Nature Communications* **2023**, *14*, 4184.
- (7) Lee, I.; Kang, W. T.; Shin, Y. S.; Kim, Y. R.; Won, U. Y.; Kim, K.; Duong, D. L.; Lee, K.; Heo, J.; Lee, Y. H.; Yu, W. J. Ultrahigh Gauge Factor in Graphene/MoS₂ Heterojunction Field Effect Transistor with Variable Schottky Barrier. *ACS Nano* **2019**, *13*, 8392–8400, PMID: 31241306.

- (8) Sarkar, D.; Banerjee, K. Proposal for tunnel-field-effect-transistor as ultra-sensitive and label-free biosensors. *Applied Physics Letters* **2012**, *100*, 143108.
- (9) Wilson, H. F.; Warschkow, O.; Marks, N. A.; Curson, N. J.; Schofield, S. R.; Reusch, T. C. G.; Radny, M. W.; Smith, P. V.; McKenzie, D. R.; Simmons, M. Y. Thermal dissociation and desorption of PH₃ on Si(001): A reinterpretation of spectroscopic data. *Phys. Rev. B* **2006**, *74*, 195310.
- (10) Warschkow, O.; Curson, N. J.; Schofield, S. R.; Marks, N. A.; Wilson, H. F.; Radny, M. W.; Smith, P. V.; Reusch, T. C. G.; McKenzie, D. R.; Simmons, M. Y. Reaction paths of phosphine dissociation on silicon (001). *The Journal of Chemical Physics* **2016**, *144*, 014705.
- (11) Fuechsle, M.; Miwa, J. A.; Mahapatra, S.; Ryu, H.; Lee, S.; Warschkow, O.; Hollenberg, L. C. L.; Klimeck, G.; Simmons, M. Y. A single-atom transistor. *Nature Nanotechnology* **2012**, *7*, 242–246.
- (12) Ivie, J. A.; Campbell, Q.; Koepke, J. C.; Brickson, M. I.; Schultz, P. A.; Muller, R. P.; Mounce, A. M.; Ward, D. R.; Carroll, M. S.; Bussmann, E.; Baczewski, A. D.; Misra, S. Impact of Incorporation Kinetics on Device Fabrication with Atomic Precision. *Phys. Rev. Applied* **2021**, *16*, 054037.
- (13) Wyrick, J.; Wang, X.; Namboodiri, P.; Kashid, R. V.; Fei, F.; Fox, J.; Silver, R. Enhanced Atomic Precision Fabrication by Adsorption of Phosphine into Engineered Dangling Bonds on H-Si Using STM and DFT. *ACS Nano* **2022**, *16*, 19114–19123.
- (14) Goh, K. E. J.; Oberbeck, L.; Simmons, M. Y.; Hamilton, A. R.; Butcher, M. J. Influence of doping density on electronic transport in degenerate Si:P δ -doped layers. *Phys. Rev. B* **2006**, *73*, 035401.
- (15) Weber, B.; Mahapatra, S.; Ryu, H.; Lee, S.; Fuhrer, A.; Reusch, T. C. G.; Thompson, D. L.; Lee, W. C. T.; Klimeck, G.; Hollenberg, L. C. L.; Simmons, M. Y. Ohm's Law Survives to the Atomic Scale. *Science* **2012**, *335*, 64–67.

- (16) McKibbin, S. R.; Scappucci, G.; Pok, W.; Simmons, M. Y. Epitaxial top-gated atomic-scale silicon wire in a three-dimensional architecture. *Nanotechnology* **2013**, *24*, 045303.
- (17) Keizer, J. G.; McKibbin, S. R.; Simmons, M. Y. The Impact of Dopant Segregation on the Maximum Carrier Density in Si:P Multilayers. *ACS Nano* **2015**, *9*, 7080–7084, PMID: 26083628.
- (18) Škerek, T.; Koester, S. A.; Douhard, B.; Fleischmann, C.; Fuhrer, A. Bipolar device fabrication using a scanning tunnelling microscope. *Nature Electronics* **2020**, *3*, 524–530.
- (19) Dwyer, K. J.; Baek, S.; Farzaneh, A.; Dreyer, M.; Williams, J. R.; Butera, R. E. B-Doped δ -Layers and Nanowires from Area-Selective Deposition of BCl₃ on Si(100). *ACS Applied Materials & Interfaces* **2021**, *13*, 41275–41286.
- (20) Ward, D.; Schmucker, S.; Anderson, E.; Bussmann, E.; Tracy, L.; Lu, T.-M.; Maurer, L.; Baczewski, A.; Campbell, D.; Marshall, M.; Misra, S. Atomic precision advanced manufacturing for digital electronics. *EDFAAO* **2020**, *22*, 4–10.
- (21) Wyrick, J.; Wang, X.; Kashid, R. V.; Namboodiri, P.; Schmucker, S. W.; Hagmann, J. A.; Liu, K.; Stewart Jr., M. D.; Richter, C. A.; Bryant, G. W.; Silver, R. M. Atom-by-Atom Fabrication of Single and Few Dopant Quantum Devices. *Advanced Functional Materials* **2019**, *29*, 1903475.
- (22) Mahapatra, S.; Büch, H.; Simmons, M. Y. Charge Sensing of Precisely Positioned P Donors in Si. *Nano Letters* **2011**, *11*, 4376–4381, PMID: 21919458.
- (23) House, M. G.; Peretz, E.; Keizer, J. G.; Hile, S. J.; Simmons, M. Y. Single-charge detection by an atomic precision tunnel junction. *Applied Physics Letters* **2014**, *104*, 113111.
- (24) Donnelly, M. B.; Keizer, J. G.; Chung, Y.; Simmons, M. Y. Monolithic Three-Dimensional Tuning of an Atomically Defined Silicon Tunnel Junction. *Nano Letters* **2021**, *21*, 10092–10098, PMID: 34797661.

- (25) Fricke, L.; Hile, S. J.; Kranz, L.; Chung, Y.; He, Y.; Pakkiam, P.; House, M. G.; Keizer, J. G.; Simmons, M. Y. Coherent control of a donor-molecule electron spin qubit in silicon. *Nature Communications* **2021**, *12*, 3323.
- (26) Wang, X.; Khatami, E.; Fei, F.; Wyrick, J.; Namboodiri, P.; Kashid, R.; Rigosi, A. F.; Bryant, G.; Silver, R. Experimental realization of an extended Fermi-Hubbard model using a 2D lattice of dopant-based quantum dots. *Nature Communications* **2022**, *13*, 6824.
- (27) Mendez, J. P.; Mamaluy, D. Uncovering anisotropic effects of electric high-moment dipoles on the tunneling current in δ -layer tunnel junctions. *Scientific Reports* **2023**, *13*, 22591.
- (28) Li, J.; Zhang, Y.; To, S.; You, L.; Sun, Y. Effect of Nanowire Number, Diameter, and Doping Density on Nano-FET Biosensor Sensitivity. *ACS Nano* **2011**, *5*, 6661–6668, PMID: 21815637.
- (29) Mamaluy, D.; Mendez, J. P.; Gao, X.; Misra, S. Revealing quantum effects in highly conductive δ -layer systems. *Communications Physics* **2021**, *4*, 205.
- (30) Mendez, J. P.; Mamaluy, D. Conductivity and size quantization effects in semiconductor δ -layer systems. *Scientific Reports* **2022**,
- (31) Kiyama, H.; Korsch, A.; Nagai, N.; Kanai, Y.; Matsumoto, K.; Hirakawa, K.; Oiwa, A. Single-electron charge sensing in self-assembled quantum dots. *Scientific Reports* **2018**, *8*, 13188.
- (32) Averin, D.; Likharev, K. Coulomb blockade of single-electron tunneling, and coherent oscillations in small tunnel junctions. *J Low Temp Phys* **1986**, *63*, 345–373.
- (33) Keldysh, L. V. Diagram Technique for Nonequilibrium Processes. *Sov. Phys. J. Exp. Theor. Phys.* **1965**, *20*, 1018.
- (34) Datta, S. *Electronic transport in mesoscopic systems*; Cambridge university press, 1997.

- (35) Mamaluy, D.; Sabathil, M.; Vogl, P. Efficient method for the calculation of ballistic quantum transport. *J. Appl. Phys.* **2003**, *93*, 4628–4633.
- (36) Mamaluy, D.; Mannargudi, A.; Vasileska, D.; Sabathil, M.; Vogl, P. Contact block reduction method and its application to a 10 nm MOSFET device. *Semiconductor Science and Technology* **2004**, *19*, S118–S121.
- (37) Sabathil, M.; Mamaluy, D.; Vogl, P. Prediction of a realistic quantum logic gate using the contact block reduction method. *Semiconductor Science and Technology* **2004**, *19*, S137–S138.
- (38) Mamaluy, D.; Vasileska, D.; Sabathil, M.; Zibold, T.; Vogl, P. Contact block reduction method for ballistic transport and carrier densities of open nanostructures. *Phys. Rev. B* **2005**, *71*, 245321.
- (39) Khan, H. R.; Mamaluy, D.; Vasileska, D. Quantum Transport Simulation of Experimentally Fabricated Nano-FinFET. *IEEE T. Electron Dev.* **2007**, *54*, 784–796.
- (40) Khan, H. R.; Mamaluy, D.; Vasileska, D. 3D NEGF quantum transport simulator for modeling ballistic transport in nano FinFETs. *Journal of Physics: Conference Series* **2008**, *107*, 012007.
- (41) Gao, X.; Mamaluy, D.; Nielsen, E.; Young, R. W.; Shirkorshidian, A.; Lilly, M. P.; Bishop, N. C.; Carroll, M. S.; Muller, R. P. Efficient self-consistent quantum transport simulator for quantum devices. *J. Appl. Phys.* **2014**, *115*, 133707.
- (42) Mendez, J. P.; Mamaluy, D.; Gao, X.; Misra, S. Quantum Transport Simulations for Si:P δ -layer Tunnel Junctions. 2021 International Conference on Simulation of Semiconductor Processes and Devices (SISPAD). 2021; pp 210–214.
- (43) Mendez, J. P.; Mamaluy, D.; Gao, X.; Anderson, E. M.; Campbell, D. M.; Ivie, J. A.; Lu, T.-M.; Schmucker, S. W.; Misra, S. Quantum Transport in Si:P δ -Layer Wires. 2020 Interna-

- tional Conference on Simulation of Semiconductor Processes and Devices (SISPAD). 2020; pp 181–184.
- (44) Goh, K. E. J.; Simmons, M. Y. Impact of Si growth rate on coherent electron transport in Si:P delta-doped devices. *Appl. Phys. Lett.* **2009**, *95*, 142104.
- (45) Reusch, T. C. G.; Goh, K. E. J.; Pok, W.; Lo, W.-C. N.; McKibbin, S. R.; Simmons, M. Y. Morphology and electrical conduction of Si:P δ -doped layers on vicinal Si(001). *J. Appl. Phys.* **2008**, *104*, 066104.
- (46) McKibbin, S. R.; Polley, C. M.; Scappucci, G.; Keizer, J. G.; Simmons, M. Y. Low resistivity, super-saturation phosphorus-in-silicon monolayer doping. *Appl. Phys. Lett.* **2014**, *104*, 123502.
- (47) Donnelly, M. B.; Munia, M. M.; Keizer, J. G.; Chung, Y.; Huq, A. M. S.-E.; Osika, E. N.; Hsueh, Y.-L.; Rahman, R.; Simmons, M. Y. Multi-Scale Modeling of Tunneling in Nanoscale Atomically Precise Si:P Tunnel Junctions. *Advanced Functional Materials* *n/a*, 2214011.
- (48) Perdew, J. P.; Zunger, A. Self-interaction correction to density-functional approximations for many-electron systems. *Phys. Rev. B* **1981**, *23*, 5048–5079.
- (49) Mendez, J. P.; Misra, S.; Mamaluy, D. Influence of imperfections on tunneling rate in δ -layer junctions. *Phys. Rev. Appl.* **2023**, *20*, 054021.
- (50) Škerek, T.; Koester, S. A.; Douhard, B.; Fleischmann, C.; Fuhrer, A. Bipolar device fabrication using a scanning tunnelling microscope. *Nature Electronics* **2020**, *3*, 524–530.
- (51) McKibbin, S. R.; Clarke, W. R.; Fuhrer, A.; Reusch, T. C. G.; Simmons, M. Y. Investigating the regrowth surface of Si:P δ -layers toward vertically stacked three dimensional devices. *Applied Physics Letters* **2009**, *95*, 233111.

- (52) Polley, C. M.; Clarke, W. R.; Miwa, J. A.; Simmons, M. Y.; Wells, J. W. Microscopic four-point-probe resistivity measurements of shallow, high density doping layers in silicon. *Applied Physics Letters* **2012**, *101*, 262105.
- (53) Mazzola, F.; Polley, C. M.; Miwa, J. A.; Simmons, M. Y.; Wells, J. W. Disentangling phonon and impurity interactions in δ -doped Si(001). *Applied Physics Letters* **2014**, *104*, 173108.

Competing interests

The authors declare no competing interests.